Ignition thresholds of aluminized HMX-based polymer-bonded explosives

Christopher Miller[a)], Seokpum Kim[b)], Yasuyuki Horie[c)], and Min Zhou[a)],

[a)] *The George W. Woodruff School of Mechanical Engineering, Georgia Institute of Technology, Atlanta, Georgia 30332-0405, USA;*
[b)] *Oak Ridge National Laboratory, P.O. Box 2008, Oak Ridge, TN 37831, USA*
[c)] *(ret.) Air Force Research Lab, Munitions Directorate, 2306 Perimeter Road, Eglin AFB, Florida 32542, USA*

The ignition of aluminized HMX-based polymer-bonded explosives (PBXs) under shock loading is studied via mesoscale simulations. The conditions analyzed concern loading pulses of 20 nanoseconds to 0.8 microseconds in duration and impact piston velocities on the order of 400-1000 m/s or loading stresses on the order of 3-14 GPa. The sets of samples studied have stochastically similar microstructures consisting of a bimodal distribution of HMX grains, an Estane binder, and aluminum particles 50-100 μm in diameter. The computational model accounts for constituent elasto-vicoplasticity, viscoelasticity, bulk compressibility, fracture, interfacial debonding, internal contact, bulk and frictional heating, and heat conduction. The analysis focuses on the development of hotspots under different material settings and loading conditions. In particular, the ignition thresholds in the forms of the James relation and the Walker-Wasley relation and the corresponding ignition probability are calculated and expressed as fucntions of the aluminum volume fraction for the PBXs analyzed. It is found that the addition of aluminum raises the ignition thresholds, causing the materials to be less sensitive. Dissipation and heating mechanism changes responsible for this trend are delineated.

1. Introduction

Understanding the physical mechanisms governing the ignition behavior of high explosives (HEs) is a critical challenge when designing insensitive munitions. One of the predominant theories regarding detonation correlates ignition with the development of critical hotspots in an energetic sample under loading [1-4]. A hotspot, or a localized temperature spike, is assumed to reach criticality when the heat generation from the exothermic chemical decomposition of the energetic material into its product gases outpaces the heat dissipation due to conduction [5]. Microstructure plays a dominant role in the formation of hotspots. Material attributes, including defects, porosity, grain size distribution, can all play a role in localized energy dissipation under shock loading [6-8]. The mechanisms behind the development of these critical hotspots, and resulting ignition, is an important topic of research in the field of energetic materials, and currently requires theoretical/simulation approaches to study effectively, as direct experimental measurement of localized heating at the level of individual hotspots remains largely elusive and is only in its infancy.

A common practice in designing high-performance insensitive energetic materials is to incorporate initially inert constituents, which serve as fuel following detonation, but does not directly participate in the detonation process. Aluminum is one such constituent and is commonly combined with a mixture of energetic grains and some form of polymer binder to form an aluminized polymer-bonded explosive (APBX) [9, 10]. Aluminum was first patented to increase explosive performance by Roth in 1900 [11], and over time experiments have optimized the volume fraction of aluminum required to maximize explosive power [12] at around 20%. Experiments show that the addition of aluminum particles decreases detonation velocity while increasing the chemical reaction time [9]. The heat of explosion also increases as aluminum is introduced, which allows the explosive to maintain its total output power while still being less sensitive to ignition [13]. The localized mechanical effects of aluminum particles in PBX during shock loading have yet to be thoroughly analyzed. Since hotspots are localized phenomena, understanding the effects of aluminum and how it interacts with energetic granules on a microscale is critical to the development of insensitive energetic materials. So far, there is a lack of systematic and quantitative study on the effects of aluminum on the ignition and detonation behaviors of polymer-bonded explosives (PBXs).

In this paper, we quantify the effects of aluminization by simulating the thermomechanical processes in the microstructures of PBXs under shock loading from impact by thin flyers using a recently developed Lagrangian cohesive finite element method (CFEM) [14-17]. The focus is on the ignition behavior. The PBXs studied are a combination of Octahydro-1,3,5,7-tetranitro-1,3,5,7-tetrazocine (HMX) grains, Estane binder, and Al 7570 alloy particles. The CFEM model accounts for constituent elasto-vicoplasticity, viscoelasticity, bulk compressibility, fracture, interfacial debonding, internal contact, bulk and frictional heating, and heat conduction. This framework allows for explicit tracking of frictional heating, which is an often overlooked source of

heat generation in many models and codes and can significantly affect the generation of hotspots in fully packed HMX [8] and PBXs [14, 18, 19]. The formation of hotspots is extremely microstructure-dependent. In this study, multiple samples are analyzed in order to represent the natural stochasticity present in real experimental microstructures. Each sample sets have aluminum concentrations of 0%, 6%, 10%, and 18% by volume. The volume fraction of the polymer binder is 19% in all cases, and the remaining volume of the microstructures are occupied by a bimodal distribution of randomly distributed HMX grains. This bimodal size distribution of HMX grains include both large and small grains similar to those commonly seen in PBXs in experiments. At different stages of shock loading, analyses are carried out to identify critical hotspots using a recently developed ignition criterion that factors in hotspot size and temperature distribution and accounts for thermal and chemical effects [17]. If a specified critical hotspot density threshold is exceeded, the sample is assumed to reach criticality.

As far as what can be found in the open literature, the first reported attempt to quantitatively characterize the desensitization effect of aluminum on the ignition of aluminized PBX [20] focused on delineating the relative importance of each heating mechanism by directly correlating the loading conditions with time to criticality after onset of loading. While the analysis is insightful, the use of the time to criticality as the measure for material behavior represents only an indirect approach as this quantity is not directly measurable in experiments and is not normally used in application. Here, we adopt a more direct approach by using a probabilistic ignition criterion in the forms of the modified James criterion proposed by Gresshoff and Hrousis [21] and Welle et al. [22] and the Walker-Wasley criterion [23]. Since the criteria use macroscopically measurable quantities that are routinely used in engineering and material analyses, the current paper can be regarded as, as far as we are aware of, the first successful attempt at linking the microstructural attributes of APBXs to practically useful engineering performance measures. Furthermore, quantitative analytical expressions for the probability of ignition as functions of loading are explicitly established. Conversely, these relations also yield the macroscopic ignition thresholds in the James space and Walker-Wasley space for any given level of ignition probability. It is important to note that this analysis only examines the hotspot heating up until the point of criticality; it is not our focus to analyze the subsequent effects of chemistry following hotspot criticality and the resulting thermal explosion. By definition, once a hotspot reaches criticality, the heat generation due to chemistry occurs more rapidly than heat loss due to conduction which implies the sample will eventually reach ignition. Studying the governing physics leading to hotspot criticality is sufficient for the sensitivity analysis presented in this work. Future work studying the effects of hotspots post criticality, including the entire shock to detonation (SDT) spectrum will be the subject of a separate paper.

2. Framework of Analysis

In this analysis, we focus on the ignition behavior of aluminized HMX-based PBX under shock pulse loading. The microstructure generation, physical models, and initiation prediction models are outlined in this section.

2.1. Microstructure

The microstructures used in these simulations consist of HMX grains and aluminum particulates distributed in an Estane matrix. The volume fraction of the Estane binder remains a constant 19% volume fraction of an entire microstructure. The aluminum and HMX combined constitute the remaining 81% of the volume fraction in the following four concentrations: 1) 0% Al, 81% HMX; 2) 6% Al, 75% HMX; 3) 10% Al, 71% HMX; and 4) 18% Al, 63% HMX. Samples of these microstructures are on display in Fig. 1.

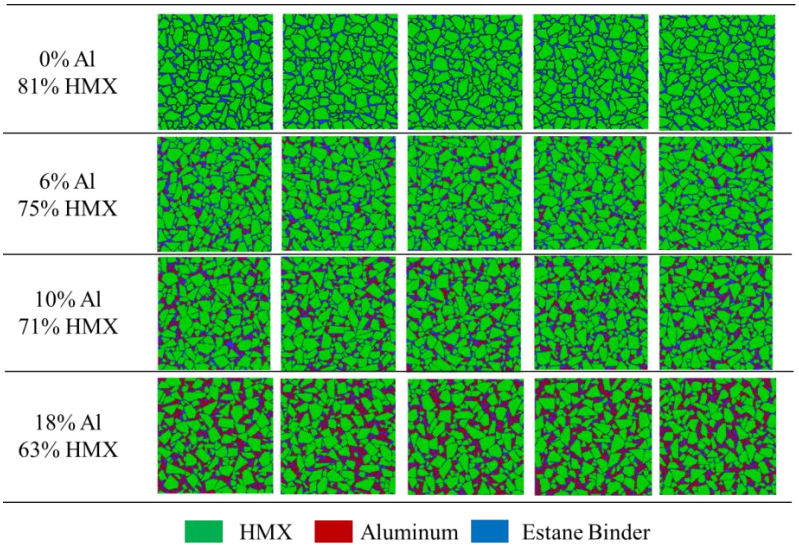

Fig. 1 – Samples of computationally generated, statistically similar microstructures for four levels of aluminization: 0 % Al, 6 % Al, 10% Al, and 18% Al. Estane binder has a constant volume fraction of 19%.

The HMX grain distribution is generated using Voronoi tessellation. Two monomodal distributions of grains are generated: one large (200-400 µm diameter) and one small (50-200 µm diameter). Appropriately sized grains from each distribution are saved to a library, and randomly redistributed into microstructures until the appropriate volume fraction of HMX is met to create a microstructure of desired attributes. In partiualr, the grains from the two monomodal distributions are combined to create microstructures with bimodal distributions of grains of different volume fractions. Following this, 50 µm diameter aluminum particles (Al 7570 alloy) are randomly inserted into the empty space not already occupied by HMX, until a total volume fraction of 81% has been achieved. Any remaining empty space is assigned to binder. This method of microstructure generation results in realistic, randomized, and stochastically similar microstructures, which allow for statistically similar testing - necessary for studying initiation probability. A statistical analysis of the stochasticity among the generated samples is presented in Fig. 2.

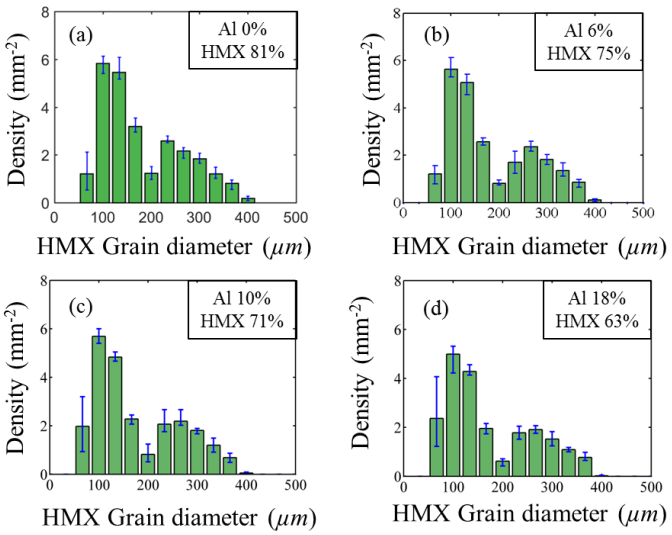

Fig. 2 – Bimodal HMX grain distributions for the samples shown in Fig. 1. The error bars indicate the maximum and minimum values among the samples in each set; (a) 0% Al; (b) 6% Al; (c) 10% Al; (d) 18% Al.

Experimental samples have inherently heterogeneous properties, including nano and micro scale voids, microcracks, and directionality of stiffness due to the anisotropic nature of the HMX crystal. The heterogeneities are phenomenologically accounted for by randomly varying the elastic modulus of the HMX grains. Both computational and experimental results have previously shown how microstructure heterogeneity and defects alter the effective elastic modulus of the grain. Yang et al. [24]

performed MD simulations of a void in a copper plate, and demonstrated a negative correlation between the elastic modulus of the plate and the volume fraction of the void. Hudson et al. [25] found that grains with higher defects have a lower elastic modulus. Using the stiffness tensor provided by Sewell et al. [26], the minimum, maximum, and Voigt-Reuss-Hill average of the Young's modulus are calculated to be 12.9, 30.3, and 20.0 GPa respectively. Each HMX grain is randomly assigned one of these values. For simplicity, the aluminum particles are assumed to be homogeneous and isotropic. For the purposes of this study, no initial interfacial defects in the forms debonding between different constituents are considered.

2.2. Loading Configurations

The specimen is initially stress-free and at rest. Impact loading is effected by applying a short-duration velocity on the top boundary of the sample. The left and right boundaries are constrained such that lateral expansion does not occur. This is a 2D model and the conditions of plane-strain are applied. The pulse intensity (U_P) and duration (t_{pulse}) are chosen to represent the loading characteristics of given combinations of flyer velocity and thickness. For simplicity, a single imposed velocity is applied on the top of the sample for the specified pulse width (see Fig. 3(a)). In real PBX microstructures, different materials have varying impedances, which would lead to non-uniform velocities along the sample boundary from a single flyer. This discrepancy is assumed negligible when the flyer and the confinement materials are significantly harder that the PBX. The specific loading conditions used in the computational analysis are the particle velocities of $U_{\text{p}} = 400, 500, 600, 800, 1000\,\text{m/s}$ and the pulse duration of $t_{\text{pulse}} = 40 - 640\,ns$, as listed in Table I. For each velocity, seven different pulse durations are applied to each sample, yielding 700 microstructure - loading combinations (5 velocities × 7 pulse durations × 4 aluminum concentrations × 5 samples). The shock pulse profile imparted onto the sample at the upper boundary is shown in Fig. 3(b). The velocity increases from $0\,\text{m/s}$ to U_{p} over the period of a 10 ns ramp time. This velocity is maintained until the downward ramp is reached at t_{ramp2}, after which the pulse velocity linearly decreases to zero over the course of 10 ns. After the final time, τ, the velocity constraint is removed. The side boundaries are constrained in the *x*-direction, while the bottom boundary is constrained in the *y*-direction. These three boundaries serve as frictionless walls during the simulation.

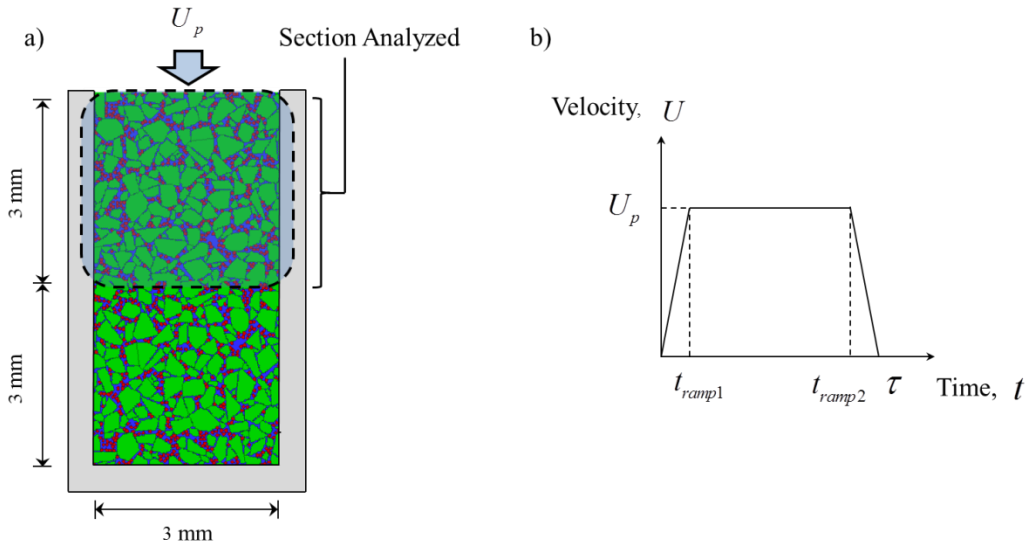

Fig. 3 – (a) Loading configuration of an arbitrary microstructure sample with an imposed particle velocity of U_p at the upper end. Only the top half of the sample traversed by the downward stress wave is analyzed to avoid the effects of wave reflection. (b) Particle velocity profile imposed with a magnitude of U_p for a pulse duration of τ. In all cases, t_{ramp1} = 10 ns and t_{ramp2} = (τ -10 ns).

Table I. Specific loading conditions

% Al / U_p	400 m/s	500 m/s	600 m/s	800 m/s	1000 m/s
0% Al	520 – 640 ns	220 - 340 ns	130 – 190 ns	50 – 110 ns	40 – 70 ns
6% Al	520 – 640 ns	220 - 340 ns	130 – 190 ns	50 – 110 ns	40 – 70 ns
10% Al	520 – 640 ns	220 - 340 ns	130 – 190 ns	50 – 110 ns	40 – 70 ns
18% Al	520 – 640 ns	220 - 340 ns	130 – 190 ns	50 – 110 ns	40 – 70 ns

2.3. Constitutive Relations

The computational analysis is performed using CODEX (Cohesive Dynamics for Explosives), a recently developed Lagrangian cohesive finite element code. This framework accounts for the dominant thermo-mechanical processes including constituent elasto-vicoplasticity, viscoelasticity, bulk compressibility, fracture, interfacial debonding, internal contact, bulk and frictional heating, and heat conduction. The aluminum follows the same constitutive model as the HMX grains, and uses different material parameters. It is assumed HMX grains and the Al particles undergo elasto-viscoplastic deformations. A detailed description of the constitutive models used is in Ref. [8]. The viscoplastic relations take into account strain hardening as well as the strain rate dependence. Table II and Table III detail the material parameters used for the viscoplastic relation of HMX and aluminum respectively. The evolution of the hydrostatic part of the stress tensor is governed by a Birch-Murnaghan equation of state. Details regarding the binder constitutive model, including the parameters and calibration techniques used in this simulation, can be found in reference [16]

Table II. HMX material parameters for viscoplastic constitutive behavior

σ_0 (MPa)	ε_0	N	T_0 (K)	β
260	5.88×10^{-4}	0.0	293	0.0
$\dot{\bar{\varepsilon}}_0$ (s^{-1})	m	$\dot{\bar{\varepsilon}}_m$ (s^{-1})	a (1/MPa)	κ
1×10^{-4}	100.0	8.0×10^{12}	22.5	0.0

Table III. Al 7570 material parameters for viscoplastic constitutive behavior

σ_0 (MPa)	ε_0	N	T_0 (K)	β
415	6×10^{-3}	0.07	293	0.035
$\dot{\bar{\varepsilon}}_0$ (s^{-1})	m	$\dot{\bar{\varepsilon}}_m$ (s^{-1})	a (1/MPa)	κ
1×10^{-4}	50.0	8.0×10^{8}	5	3.0

2.4. Cohesive Element Framework

The fracture of the microstructure under high-impact loading is modeled using a cohesive finite element framework. The fracture follows a bilinear traction separation law (Fig. 4) outlined below. Until the displacement (δ) between two bulk elements reaches a critical distance (δ_0), the cohesive elements are considered elastic. Once this critical displacement is exceeded, the cohesive element will begin to lose energy, and a resulting reduction in element stiffness occurs. If the element passes a second critical displacement (δ_c), the total energy lost equals the critical energy release rate and the interface between its two connecting bulk elements is considered fractured. Once this point is reached, the strength parameters of the cohesive element connecting the two bulk elements are set to zero. The cohesive parameter values for HMX, Estane, and aluminum are listed in Table IV. These cohesive elements allow for arbitrary crack initiation and propagation, while also giving CODEX the ability to explicitly

model initial debonding between grains and binder, commonly observed in experimental samples. The effect of initial debonding on ignition sensitivity is outside the scope of this paper and will be studied in future work. Further details on this cohesive model can be found in reference [16].

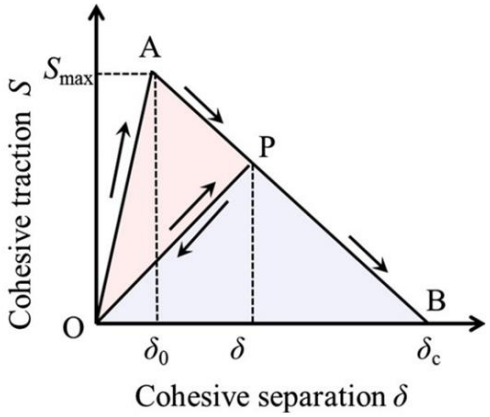

Fig. 4 – Bilinear traction-separation law for potential cracks.

Table IV. Cohesive Relation Parameters

Element Type	δ_c (μm)	δ_0(μm)	S_{max} (MPa)
Estane-Estane	10	0.1	557
HMX-HMX	5.0	0.005	101
Al-Al	15.4	0.0154	345
HMX-Al	4.66	0.00466	70
Al-Estane	4.71	0.00471	70
HMX-Estane	4.62	0.00924	35

2.5. Hotspot Characterization

An ignition criterion developed by Barua et al. [17] is used in this study to provide a standard for determination of hotspot criticality. This criterion assumes that a hotspot reaches criticality if its rate of heat generation by means of chemical decomposition exceeds the rate of heat lost to its surrounds, primarily through conduction. For this to occur, a certain amount of thermal energy is required to overcome the activation energy of the chemical decomposition. When a hotspot reaches a certain temperature, there is a minimum diameter it must have in order to obtain the necessary energy. If any part of the hotspot exceed this critical diameter, d_c, during the simulation, the hotspot is treated as a critical hotspot. This condition is represented by Eq. (1).

$$d(T) \geq d_c(T), \tag{1}$$

If two or more hotspots in a 3 mm^2 domain reach criticality, the entire sample is assumed to proceed to ignition. This hotspot density threshold for ignition (0.22 mm^2) was chosen based on the work of Barua et al., and further information can be found in Ref. [17].

3. Results and Discussion

A systematic quantification of the ignition of aluminized PBX is carried out, focusing on the shock intensity and shock pulse duration. Five samples of each aluminum concentration are tested at various loading intensities and pulse durations in order to determine the 50% ignition threshold. This threshold is modeled using a modified James relation in addition to a modified Walker-Wasley relation, and a probability spectrum is quantified by introducing the James number, *J*, first proposed by Gresshoff and Hrousis [21] and Walker Wasley number, *W*, first proposed by Kim et al [6]. The physical mechanisms responsible for the decreased sensitivity to ignition in samples with higher aluminum concentrations are delineated in section 3.3.

3.1. Ignition Sensitivity Threshold

The ignition threshold of PBX is fit using two models, the modified Hugh James relation and the modified Walker-Wasley relation. Each model provides a different way of understanding the ignition sensitivity of energetic materials using different loading parameters. It is possible to derive an equivalent James relation from the Walker-Wasley relation. This derivation can be found in the appendix of reference [8]

3.1.1 Hugh James Ignition Threshold

The critical energy threshold is analyzed using the hotspot ignition criterion introduced in Sec. 2.5. Fig. 5 shows the minimum energy required for ignition from five samples subjected to various shock intensities. The shock intensities are represented in a power flux form, Π , which is calculated as

$$\Pi = PU_p, \tag{2}$$

where P is the average hydrostatic part of the stress tensor at the impact face, and U_p is the particle velocity at the impact face. The energy fluence, $E = \int_0^t \Pi \, dt$, represents the total energy transferred to the material by the shock loading per unit area of the impact face. For each loading velocity tested, the power flux is found to be nearly constant, while each successive test was carried out with an incrementally higher energy fluence, which is analogous to impacting the samples with increasingly thicker flyers at the same velocity. The red circles in Fig. 5 represent samples that did not achieve criticality, and the black crosses represent samples that did reach criticality. The 50% ignition probability data points were calculated by averaging the energy fluences required for two and three samples to reach criticality for a given power flux.

Due to the stochastic nature of the random microstructures, each sample requires a different amount of minimum energy to ignite. A common way to model the probabilistic nature of the ignition behavior is to consider the 50% ignition threshold. Take the James relation [27], which is based on a minimum critical energy required for ignition, as example first here. Gresshoff and Hrousis [21] expanded on the James relation by introducing a James number, *J*, which allows for extrapolation of the ignition probability above and below the 50% threshold. The form of the modified James relation is

$$\frac{1}{J} = \frac{E_c}{E} + \frac{P_c}{P}, \tag{3}$$

where E_c and Π_c are fitting parameters which represent asymptotic thresholds for the critical energy and the critical power flux, respectively. This relation originates from the James relation [27], but uses the power flux ($\Pi = PU_p$) introduced by Welle et al. [22] to replace the specific kinetic energy ($\Sigma = 0.5U_p{}^2$). By definition, the threshold where 50% of the samples ignite (i.e. 50% probability of ignition) occurs when $J = 1$. Any combination of power flux and energy fluence above the threshold ($J > 1$) would lead to a greater than 50% probability of ignition. Similarly, any combination of power flux and energy fluence below the threshold ($J < 1$) would lead to a probability ignition less than 50%. A similar probabilisitc quantification can be carried out using the modified Walker-Wasley relation in the pressure-loading pulse duration (P-τ) space [23], as discussion later.

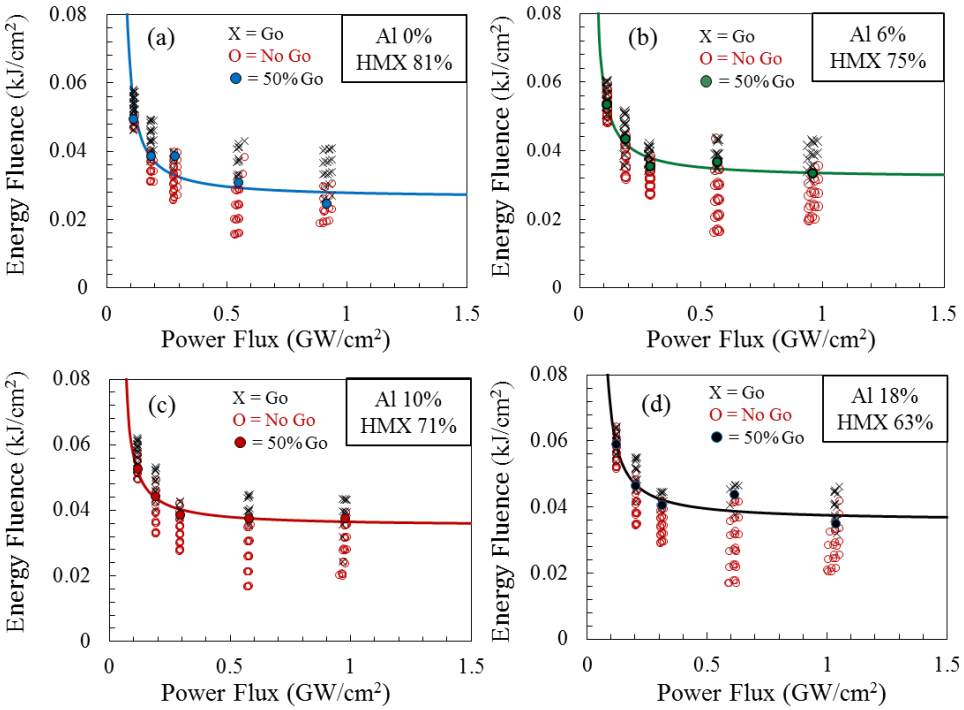

Fig. 5 – go/no go results of individual samples of APBX with different levels of aluminum: (a) 0% Al; (b) 6% Al; (c) 10% Al; (d) 18% Al.

The 50% ignition thresholds for all aluminum concentrations (0%, 6%, 10%, and 18% aluminum by volume) are shown in Fig. 6, and the corresponding parameters for the modified James relation are listed in Table V. For any given microstructure, a higher loading rate (power flux) corresponds to a lower energy fluence for ignition. As the aluminum concentration increases, the energy fluence required for 50% of the samples to reach criticality also increases, demonstrating that adding aluminum reduces the overall sensitivity of the PBX to ignition. This trend matches the experimental observations of the relative sensitivity of aluminized PBX as compared to non-aluminized PBX of Prakash et al., who measured the relative sensitivities using the standard fall hammer method [10]. Table V presents a clear trend of increasing critical energy fluence as the volume fraction of aluminum increases, however the trend in the power flux parameter is not monotonous. This is explained by the relatively fewer 50% ignition sensitivity data points available to fit the vertical asymptote at lower impact velocities, as calculations at a lower piston velocities require extremely long computation times.

The ignition sensitivities are easily distinguished at high power fluxes, and relatively indistinguishable at lower power fluxes. As the aluminum concentration increases the variation in energy fluence required for ignition decreases, which may imply there is an optimal volume fraction of aluminum that corresponds to a minimized sensitivity for ignition while maximizing power output. Various experiments testing TNT/HMX/RDX based PBXs have suggested 15-20% aluminum as an optimal amount to maximize explosive power due Al increasing the heat of explosion while decreasing the volume of gaseous products [12]. This phenomena will be the objective of a future study.

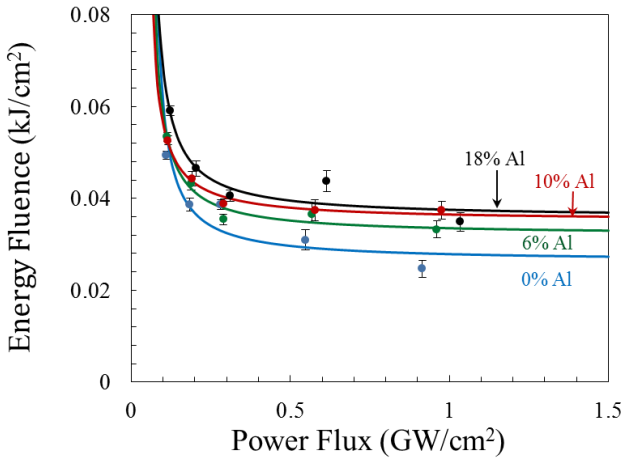

Fig. 6 – 50% ignition thresholds of APBX with different levels (0%, 6%, 10%, 18%) of aluminization analyzed in the James space.

Table V. Modified James Parameter values from Fig. 6

Aluminum Volume Fraction	E_c (kJ/cm^2)	Π_c (GW/cm^2)
0% Al	0.0263	0.0570
6% Al	0.0320	0.0452
10% Al	0.0351	0.0376
18% Al	0.0357	0.0479

3.1.2 Walker-Wasley Ignition Threshold

An alternative method of mapping the ignition threshold uses the Walker-Wasley relation [23]. First proposed in 1969, the Walker-Wasley relation uses a power law fitting to relate the average hydrostatic part of the input stress (P) and pulse duration (τ) required to reach ignition. A modified form of this relation is

$$\frac{P^n \tau}{C} = W, \tag{4}$$

where C is a material-dependent parameter and the exponential fitting parameter, n, is often set to the value of 2. This relationship provides a non-dimensional Walker-Wasley number, W, which relates to the probability of ignition. Similar to the J parameter in Eq. (3), W =1 represents the threshold where 50% of the samples reach ignition. W >1 and W <1 correspond to ignition probabilities greater than 50% and less than 50%, respectively.

The aluminized PBX initiation data is fit to the Walker-Wasley relation (Eq. (4)) in the P-τ space and the result is shown in Fig. 7. The corresponding paramters used are listed in Table VI. As the volume fraction of aluminum increases, material-dependent parameter C also increases, indicating a lower sensitivity to ignition under similar loading conditions. At lower load intensities, the Walker-Wasley fits, when ploted on the log-log scale, do not distinguish the cases for different aluminum levels as well as the Hugh James relation.

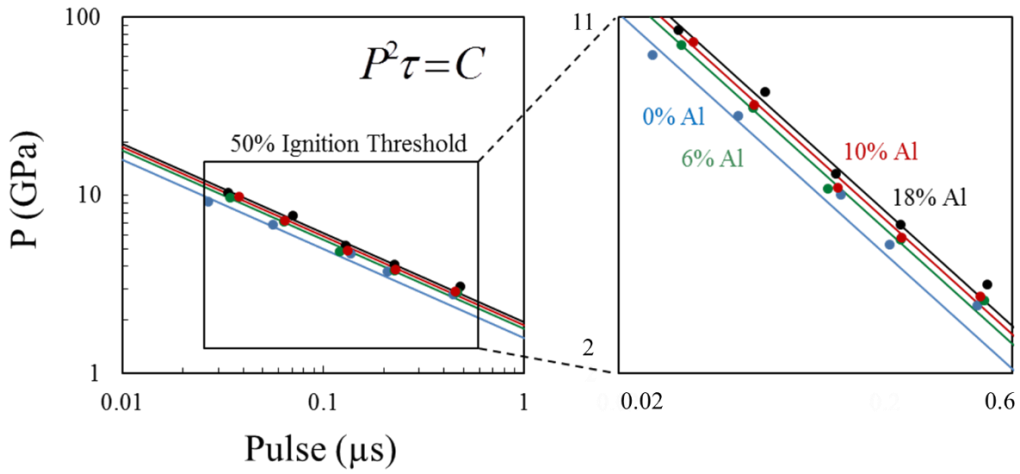

Fig. 7 – 50% ignition thresholds of APBX with different levels (0%, 6%, 10%, 18%) of aluminization analyzed in the Walker-Wasley space

Table VI. Walker-Wasley Parameter values from Fig. 7

Aluminum Volume Fraction	*C*	*W*
0% Al	2.507	1
6% Al	3.187	1
10% Al	3.489	1
18% Al	3.781	1

3.2. Ignition Probability Mapping

For the 50% ignition probability analysis above, *J* is taken to be 1 in the Hugh James space and Eq. (3), with the understanding that if *J* is greater than or less than 1, the corresponding probability of ignition is greater than or less than 50%, respectively. The probability of ignition as a function of *J* is shown in Fig. 8(a). By the same token, using the Walker-Wasley framework, the results of the ignition probability as a fucntuion of *W* is shown in Fig. 8(b).

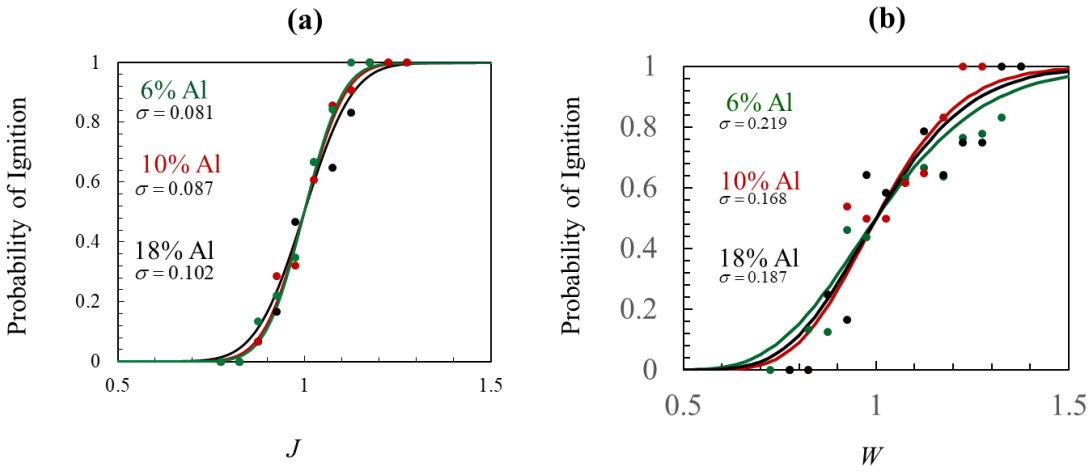

Fig. 8 – Ignition probability as a function of *J* (a) and *W* (b) for APBX with different levels of aluminization, shown in terms of the cumulative distribution function (CDF) of the Gaussian distrition.

The relationship between the probability of ignition and J is fit using a cumulative Gaussian distribution, with a mean value of $J=1$. The standard deviations σ = 0.081, 0.087, 0.102 for sample sets with 6%, 10%, and 18% of aluminum, respectively. Written in terms of the loading parameters in the James space, the igniton probability is

$$\mathcal{P}(E,\Pi)=\frac{1}{2}+\frac{1}{2}\mathrm{erf}\left[\frac{1}{\sqrt{2}\sigma}\left(\frac{E\Pi}{E_c\Pi+\Pi_c E}-1\right)\right], \tag{5}$$

where erf (·) is the error function. In the Walker-Wasley space, the probability of ignition as a function of W with a mean of $W=1$ has the standard deviation of σ = 0.219, 0.168, 0.187 for microstructures with 6%, 10%, and 18% of aluminum, respectively. Written in terms of shock pressure, P, and pulse duration, τ, the probability of ignition has the form

$$\mathcal{P}(P,\tau)=\frac{1}{2}+\frac{1}{2}\mathrm{erf}\left[\frac{1}{\sqrt{2}\sigma}\left(\ln\left(P^2\tau\right)-\ln C\right)\right], \tag{6}$$

Fig. 9 and Fig. 10 provide the probability of ignition as functions of loading in the entire loading condition spectra in the James and Walker-Wasley spaces, respectively. In each figure, the black line corresponds to all possible combinations of loading conditions where 50% of samples reach ignition. The upper and lower red dashed lines represent, respectively, the loading conditions for which 90% and 10% of samples reach ignition.

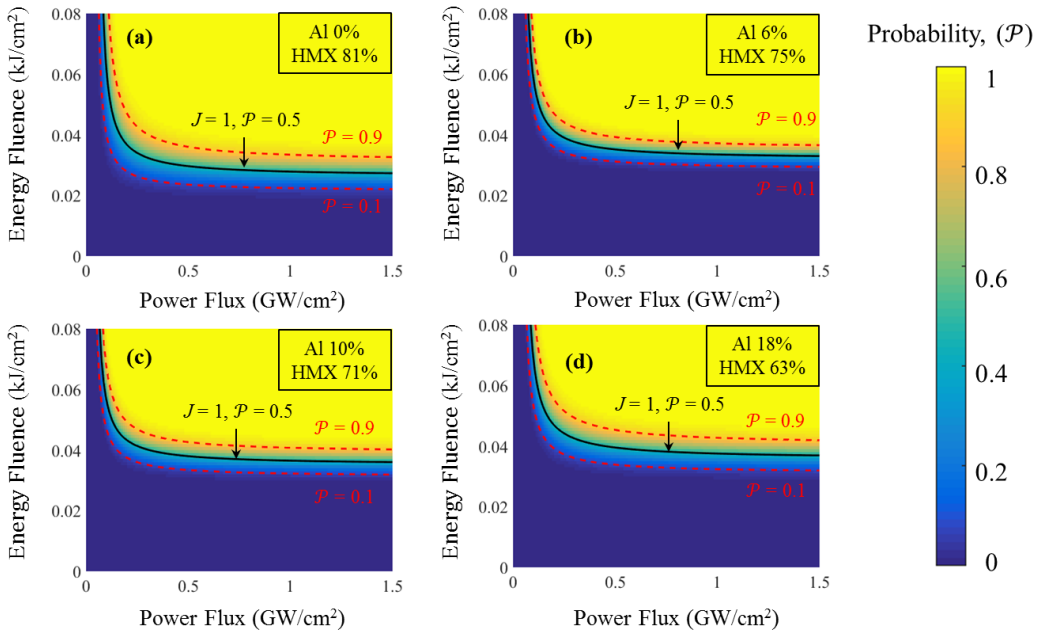

Fig. 9 – Ignition probability distribution maps for the four levels of aluminization analyzed; (a) 0% Al; (b) 6% Al; (c) 10% Al; (d) 18% Al in the energy fluence - power flux ($E-\Pi$) space.

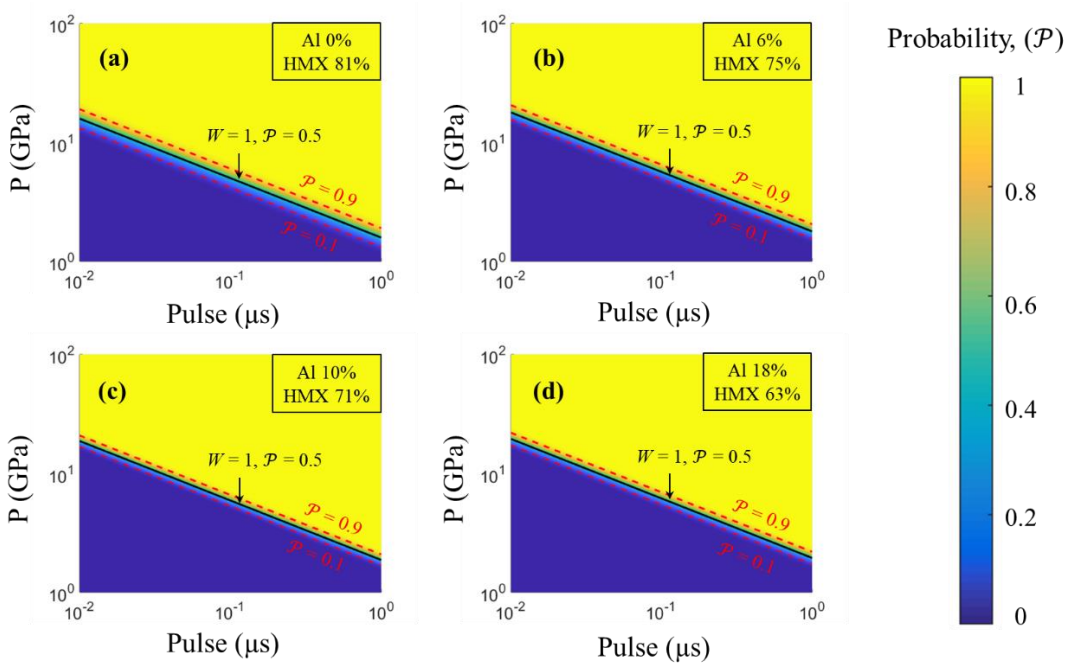

Fig. 10 – Ignition probability distribution maps for the four levels of aluminization analyzed; (a) 0% Al; (b) 6% Al; (c) 10% Al; (d) 18% Al in the pressure - pulse duration $(P-\tau)$ space.

The reason that the standard deviations of ignition probability in Fig. 8 for the different levels of aluminization are similar to each other is that the degree of microsctructure variations among the samples in the sets relative to their respective averages are similar. This can be partly seen from the similar standard deviations of grain size distributions of the samples in Fig. 2. The effect of aluminization on ignition probability is primarily on the 50% ignition thresholds, as shown in Fig. 6, Fig. 7, Fig. 9, and Fig. 10. On the otherhand, the probability spread relative to the 50% thresholds is a refelction of how different the samples in each material set are from each other. Indeed, the fact that samples of each material behave somewhat differently (statistical variations) because of inherent materials heterogeneities, and the probabilistic analyses here using J and W captures these effects. To simply put, if all samples in a material set were identical to each other (no material hetergenity, which is impossible), there wouldn't be statistical variation in behavior.

It is likely that the standard deviations of the J-$\mathcal{P}$ and W-$\mathcal{P}$ relations obtained here are smaller than what would be seen in experiments. Although the samples used in this study are statistically similar, variability among experimental samples cannot be controlled as rigidly. In addition, there are additional sources of variation in real experimental samples not explicitly modeled computationally. Specifically microstructure voids, which are known to play a significant role in the generation of hotspots, are not explicitly modeled in the scope of this paper. The incorporation of voids is part of the future work on this problem. Other factors can also contribute to measured property variations in experiments, including loading uncertainties and instrument error.

The correlation between the aluminum concentration and the modified James parameters, E_c and Π_c, as well as the modified Walker Wasley parameter, C, are shown below in Fig. 11. The data is fit to a simple linear model to outline the trend, with α being the concentration of aluminum. The resulting material parameters are listed in Table VII.

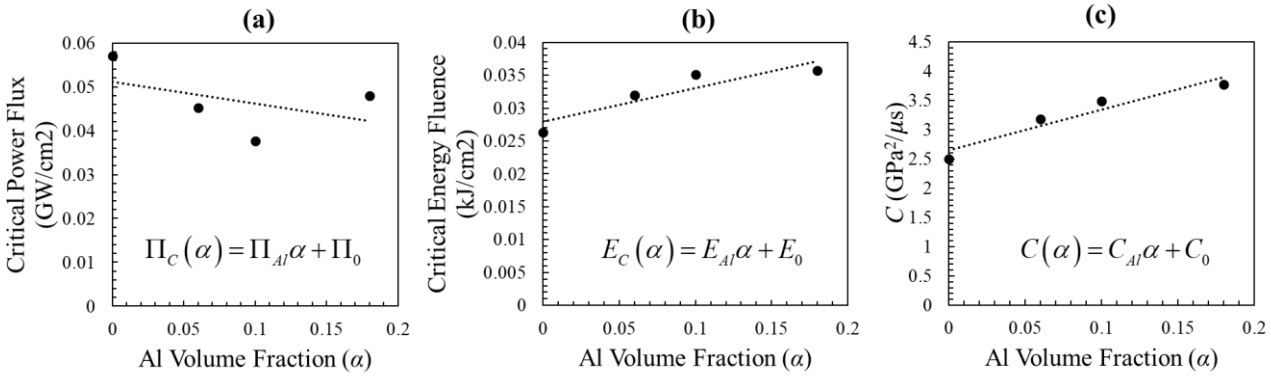

Fig. 11 – Correlation between aluminum volume fraction and (a) critical power flux, (b) critical energy fluence, and (c) material-dependent parameter *C*

Table VII. Material Properties for the linear relationships shown in Fig. 11

Material Properties	$\Pi\left(\frac{GW}{cm^2}\right)$	$E\left(\frac{kJ}{cm^2}\right)$	$C\left(\frac{GPa^2}{\mu s}\right)$
Slope	$\Pi_{Al}=-0.050$	$E_{Al}=0.052$	$C_{Al}=6.95$
Intercept	$\Pi_0=0.051$	$E_0=0.028$	$C_0=2.65$

By combining the relations above with the probability functions in Eqs. (5) and (6), we can write the probability of ignition directly as a function of the aluminum concentration, α, as well as the loading conditions as

$$\mathcal{P}(\alpha,E,\Pi)=\frac{1}{2}+\frac{1}{2}\mathrm{erf}\left[\frac{1}{\sqrt{2}\sigma}\left(\frac{E\Pi}{\Pi\left(E_{Al}\alpha+E_0\right)+E\left(\Pi_{Al}\alpha+\Pi_0\right)}-1\right)\right],\ \text{and} \tag{7}$$

$$\mathcal{P}(\alpha,P,\tau)=\frac{1}{2}+\frac{1}{2}\mathrm{erf}\left[\frac{1}{\sqrt{2}\sigma}\left(\ln\left(P^2\tau\right)-\ln\left(C_{Al}\alpha+C_0\right)\right)\right]. \tag{8}$$

Conversely, the ignition thresholds as functions of the aluminum concentration are

$$\frac{1}{J}=\frac{E_{Al}\alpha+E_0}{E}+\frac{\Pi_{Al}\alpha+\Pi_{0c}}{\Pi},\ \text{and} \tag{9}$$

$$\frac{P^2\tau}{C_{Al}\alpha+C_0}=W. \tag{10}$$

3.3. Effect of Aluminum on Hotspot Criticality

The physics governing the effect of aluminum incorporated into PBX are outlined in this section. Section 3.3.1 discusses the predominant mechanisms of heat generation, and how they are influenced by the inclusion of aluminum. Section 3.3.2 discusses the resulting effect of increasing the diameter of the aluminum particles from 50 μm to 100 μm.

3.3.1 Heat Generation in Aluminized Samples

In this analysis, three forms of heat generation due to energy dissipation are accounted for: frictional heating, plastic work, and viscous dissipation in the binder. The relative effects of frictional work and plastic work in the HMX grains are analyzed in Fig. 12. The heat generation from the viscoelastic dissipation in the binder is excluded since its contribution to heating is mostly in the Estane matrix and the effect of heat transfer via conduction is minimal in the examined time scale. It is important to study the effects of localized heat generation, rather than total heat generation, since hotspots only initialize from localized heating.

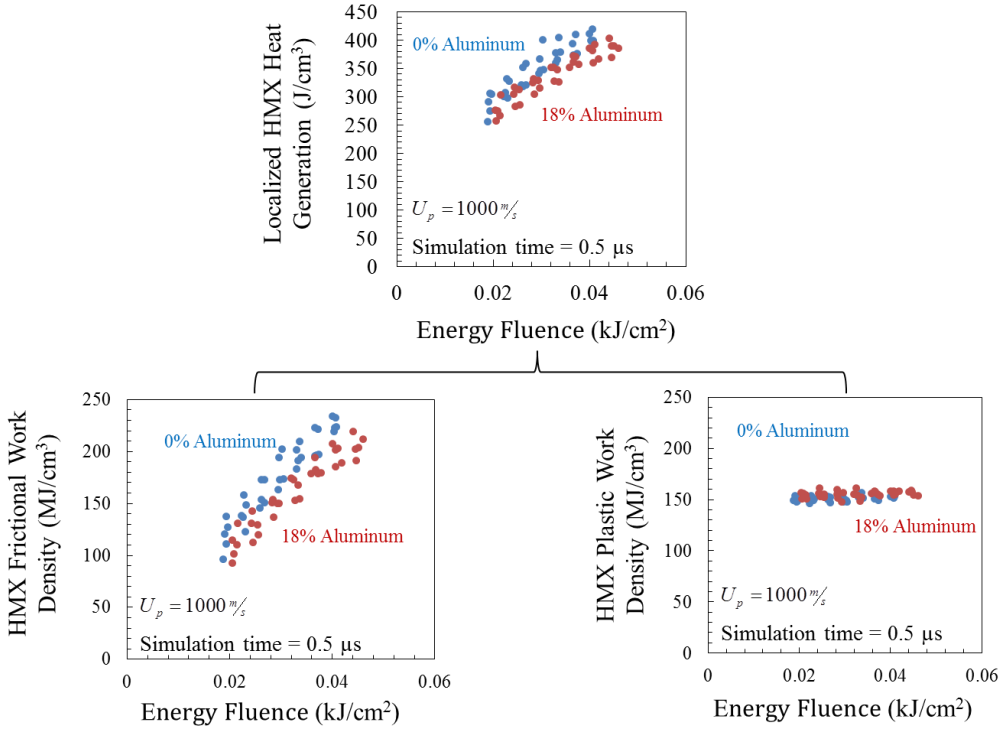

Fig. 12 - Breakdown of heat generation in HMX grains due to frictional work and plastic work

.

As seen in Fig. 12, there is a greater amount of localized heat generation in HMX grains in samples with no aluminum as compared to samples with 18% aluminum (by volume). This difference is a direct result of the increased levels of frictional work occurring in the HMX when no aluminum is present. The plastic work density and resultant heat generation from it remains relatively constant between samples regardless of the total energy fluence.

The crack density for three aluminum levels is shown in Fig. 13 for U_p = 1000 m/s. This high piston velocity is chosen because the largest difference in ignition thresholds occurs at higher power flux values. The data for 6% Al is not shown to keep the plot less cluttered and easier to visualize. As the amount of aluminum is increased, the total amount of cracking remains nearly constant (Fig. 13(a)), but the number of cracks associated with HMX decreases (Fig. 13(b)). More cracks are forming between the aluminum and the binder or between the HMX and the binder, instead of in the HMX grains in the form of intergranular cracks. Since the main source of localized heat generation is frictional dissipation stemming from fracture and subsequent material interfacial movement, this means part of the heat generation in the material is moving away from HMX, and towards the Al particles instead. This phenomenon is examined more thoroughly in section 3.3.2.

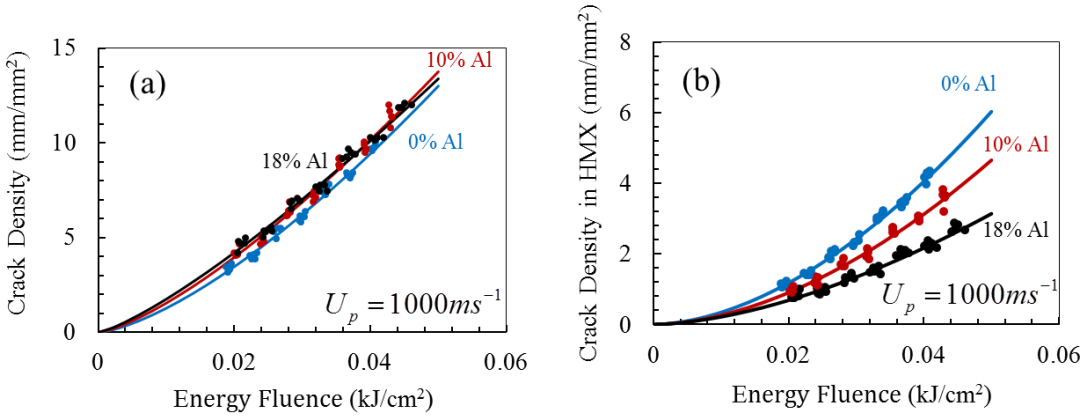

Fig. 13 - Effect of Al volume fraction on crack density in relation to the imparted energy fluence when the particle velocity is 1000 ms^{-1}; (a) total crack density; (b) density of cracks associated with HMX. The crack density in (b) has been normalized to the volume fraction of the HMX.

3.3.2 Aluminum Particle Size Effect on Initiation

In addition to the above analysis with d = 50 µm, the analysis is repeated using a larger aluminum particle diameter of d = 100 µm. In both cases, the aluminum volume fraction is constant at 10%. The results are shown in Fig. 14, with the corresponding James equation parameters listed in Table VIII. Fig. 15 shows the corresponding probability variation as J varies.

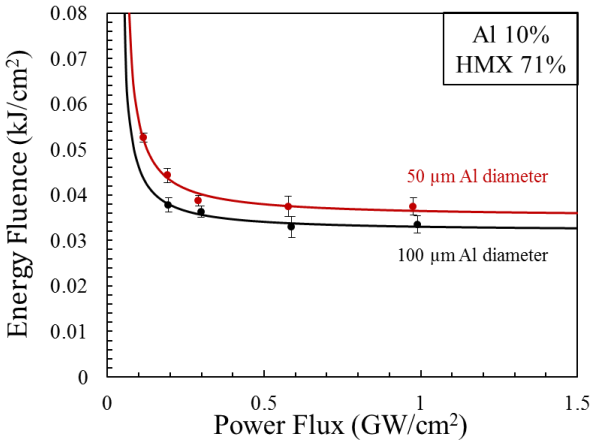

Fig. 14 – 50% ignition thresholds of 10% Al samples with 50 µm and 100 µm diameter aluminum particles.

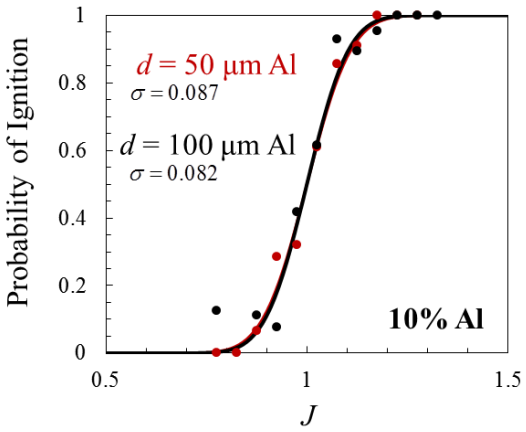

Fig. 15 – Cummulative ignition probability as a function of J for APBX with 50 and 100 μm aluminum particles. In both cases, the aluminum volume fraction is 10%.

The larger particle diameter lowers the ignition threshold and increases the ignition sensitivity. Over the entire range of input power flux analyzed (0.2 – 1 GW/cm^2), the larger aluminum particle diameter consistently corresponds to lower energy fluence for the 50% ignition threshold. This is qualitatively consisitent with experimental observations recorded by Gogulya et al. [28] showing that the detonation velocities of HMX based explosives decreased as aluminum particle size decreased (while the mass fraction of aluminum particles was held constant at 15%). As shown in Fig. 15, the variation of the ignition threshold as J varies is essentially the same for the two aluminum particle sizes. As is the case for different aluminum concentrations (volume fractions) discussed earlier, Fig. 16 does not imply that the ignition sensitivity thresholds for the two Al particle sizes are the same, but rather that the probability variations relative to the corresponding 50% thresholds essentially coincide.

First, as discussed in section 3.3.1, interfacial friction plays a more dominant role in heat generation than bulk inelastic deformation. Any fracture energy spent on crack propagation between the aluminum and binder is less energy available to the HMX grains, where the development of hotspots is key to ignition. Therefore, an increased amount of fracture on the aluminum surfaces results in desensitization. When comparing the crack density associated with aluminum particles (for both the 50 μm and 100 μm cases), over 98% of the cracks associated with aluminum are surface cracks. This implies that the total aluminum surface area has a more significant effect on sensitivity than aluminum concentration or volume fraction. Fig. 16(a) shows how the aluminum surface crack density compares between the 10% aluminum cases with large and small aluminum particle diameters. It is important to remember that no initial debonding exists in any sample. The crack density is significantly higher for the smaller particle cases, due to higher total surface area. When the total Al cracking is normalized to the total amount of Al surface area (Fig. 16(b)), the Al particle size becomes irrelevant. This evidence supports the claim that Al surface area plays a dominant role in ignition sensitivity.

The second reason why smaller aluminum particles lead to lower sensitivity to ignition is because a greater number of smaller particulates can be more spread out throughout the microstructure than fewer, larger ones. This allows for a more even dissipation of energy via aluminum debonding, which lowers the total potential energy available to the HMX phase. Since the aluminum particles are scattered randomly throughout the microstructure, decreasing their size while simultaneously increasing their quantity (to maintain the 10% Al volume fraction), increases the likelihood of an aluminum particle ending up near a potential hotspot location. The aluminum debonding can then function as an energy "sink", preventing critical temperature rise in the nearby HMX.

It is important to note that this study is only focused on the mechanical effects that lead to hotspot formation, with aluminum particles in the micron scale. It is likely that smaller aluminum particles play a larger role in detonation when chemistry is considered, especially when dealing with Al particles in the nanoscale regime, but that is outside the scope of this paper.

Table VIII. Modified James Parameter values from Fig. 11

Aluminum Diameter	E_c (kJ/cm^2)	Π_c (GW/cm^2)
50 μm	0.0351	0.0376

100 µm	0.0320	0.0306

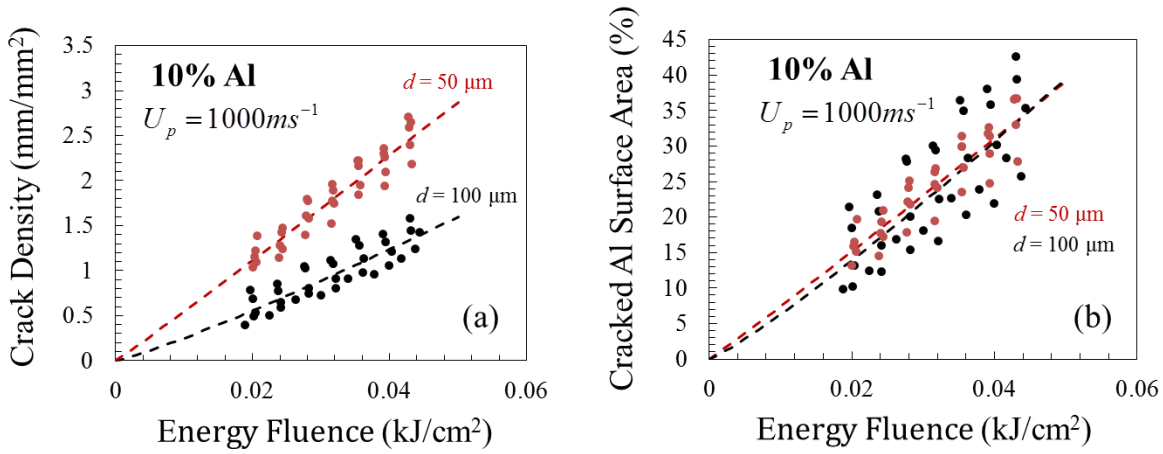

Fig. 16 – (a) Surface crack density as a function of energy fluence in 10% Al samples with 50 µm and 100 µm diameter aluminum particles. (b) Percentage of total aluminum surface area that has fractured.

3.4. Experimental Validation

So far in the open literature, there is no direct experimental measurement of the quantities predicted here. As a result, direct comparison with experiments is not possible at this time. However, general trends seen in experiments concerning the ignition and detoantion of aluminized PBX are consistent with the trends reported in this paper, as stated in the discussions above. When studying HMX samples mixed with Al and ammonium perchlorate (AP), Li et al. [29] noticed that ignition sensitivity decreased with the addition of aluminum, and concluded, "…a plentiful [amount] of Al decentralizes the impact stress on explosive, accordingly diminishes the probability of hot-spots formation. Simultaneously, a vast [amount] of Al can improve heat transmit which hamper explosion propagation from hot-spots". A number of studies report decreasing detonation velocities as the aluminum volume fraction increases. Gogulya et al. [30, 31] found that the detonation velocity decreased as the size of the aluminum particles decreased, while the volume fraction was held constant. It should be noted that nano-size aluminum particles may also significantly alter the detonation phase, which this study does not directly simulate. It is hoped that more direct experimental measurement concerning ignition thresholds will become available in the future.

4. Conclusion

The ignition behavior of APBX with microstructures containing 6%, 10%, and 18% Al by volume is analyzed and compared to that of the corresponding unaluminized PBX. The 50% ignition threshold for each Al concentration are mapped as a function of the power flux and energy fluence which are measures for loading condition. A probabilistic map is created to quantify the likelihood of ignition of the materials. The results show that, relative to the unaluminized PBX, the addition of aluminum reduces the 50% ignition threshold sensitivity by 21.7%, 33.5%, and 35.7% for APBXs with 6%, 10%, and 18% Al, respectively. In terms of the mechanisms responsible for the trend, the fictional dissipation between sliding crack surfaces plays a much more significant role in the development of critical hotspots than plastic deformation. At higher load intensities, the addition of aluminum does not significantly change the total amount of cracking in the materials, but it does encourage crack initiation in locations away from HMX, resulting in lower ignition sensitivity of the materials. The reason is that more energy is dissipated in the debonding of aluminum due to the lower cohesive strength between the Al particles and Estane binder, causing less localized heating in HMX. As the aluminum particle size is increased, the materials are more likely to generate critical hotspots for the same reason. Since larger Al particles result in less total Al surface area (as compared to an equal volume of smaller Al particles), less energy is required to debond a majority of the Al particles, allowing more cracks to form in HMX grains, leading to higher ignition sensitivity.

Finally, it is useful to point out that the goal of this paper is to illustrate the important micromechanical effects aluminum constituents have on the ignition sensitivity of PBXs. Through a thorough computational analysis, friction is identified as playing a dominant role in hotspot generation. The findings can help guide the direction of future experiments to focus on studying the importance of frictional heat dissipation under shock loading and efforts to modify the ignition sensitivity through material synthesis. A possible mechanism is to enhance the bonding strengths between different binders and constituents via design of the microstructure and change of synthesis routes. Follow-up studies in the future will examine the effects of voids in APBX and the effect of chemistry on behavior post criticality or post ignition.

5. Acknowledgements

The authors gratefully acknowledge the support from the Air Force Office of Scientific Research (Dr. Martin Schmidt) and the Defense Threat Reduction Agency (DTRA) (Dr. Douglas Allen Dalton). C. Miller acknowledges the support from the DoE NNSA Stewardship Science Graduate Fellowship Program (DENA0002135).

6. REFERENCES

1. Baer, M.R., *Modeling heterogeneous energetic materials at the mesoscale.* Thermochimica Acta, 2002. **384**(1-2): p. 351-367.
2. Bennett, J.G., et al., *A constitutive model for the non-shock ignition and mechanical response of high explosives.* Journal of the Mechanics and Physics of Solids, 1998. **46**(12): p. 2303-2322.
3. Benson, D.J. and P. Conley, *Eulerian finite-element simulations of experimentally acquired HMX microstructures.* Modelling and Simulation in Materials Science and Engineering, 1999. **7**(3): p. 333-354.
4. Rao, P.T. and K.A. Gonthier. *Analysis of Dissipation Induced by Successive Planar Shock Loading of Granular Explosive*. in *51st AIAA/SAE/ASEE Joint Propulsion Conference*. 2015. Orlando, FL.
5. Tarver, C.M., S.K. Chidester, and A.L. Nichols, *Critical conditions for impact- and shock-induced hot spots in solid explosives.* Journal of Physical Chemistry, 1996. **100**(14): p. 5794-5799.
6. Kim, S., et al., *Prediction of shock initiation thresholds and ignition probability of polymer-bonded explosives using mesoscale simulations.* Journal of the Mechanics and Physics of Solids, 2018. **114**: p. 97-116.
7. Austin, R.A., et al., *Modeling pore collapse and chemical reactions in shock-loaded HMX crystals.* Journal of Physics: Conference Series, 2014. **500**(5): p. 052002.
8. Kim, S., et al., *Computational prediction of probabilistic ignition threshold of pressed granular Octahydro-1,3,5,7-tetranitro-1,3,5,7-tetrazocine (HMX) under shock loading.* Journal of Applied Physics, 2016.
9. Antić, G. and V. Džingalašević, *Characteristics of cast PBX with aluminium.* Scientific Technical Review, 2006. **56**(3-4): p. 52-58.
10. Prakash, V., et al., *Influence of aluminium on performance of HTPB-based aluminised PBXs.* Defence Science Journal, 2004. **54**(4): p. 475-482.
11. Roth, G., *Performance of explosives*. 1900: German Patent No. 173327
12. Vadhe, P.P., et al., *Cast aluminized explosives.* Combustion Explosion and ShockWaves, 2008. **44**(4): p. 461-477.
13. Akhavan, J., *The Chemistry of Explosives*. 2004, Cambridge: The Royal Society of Chemistry.
14. Barua, A., Y. Horie, and M. Zhou, *Microstructural level response of HMX-Estane polymer-bonded explosive under effects of transient stress waves.* Proceedings of the Royal Society a-Mathematical Physical and Engineering Sciences, 2012. **468**(2147): p. 3725-3744.
15. Barua, A., et al., *Prediction of probabilistic ignition behavior of polymer-bonded explosives from microstructural stochasticity.* Journal of Applied Physics, 2013. **113**(18): p. 184907.

16. Barua, A. and M. Zhou, *A Lagrangian framework for analyzing microstructural level response of polymer-bonded explosives.* Modelling and Simulation in Materials Science and Engineering, 2011. **19**(5): p. 055001.
17. Barua, A., et al., *Ignition criterion for heterogeneous energetic materials based on hotspot size-temperature threshold.* Journal of Applied Physics, 2013. **113**(6): p. 064906.
18. Barua, A., Y. Horie, and M. Zhou, *Energy localization in HMX-Estane polymer-bonded explosives during impact loading.* Journal of Applied Physics, 2012. **111**(5): p. 054902.
19. Barua, A. and M. Zhou, *Computational analysis of temperature rises in microstructures of HMX-Estane PBXs.* Computational Mechanics, 2013. **52**(1): p. 151-159.
20. Kim, S., Y. Horie, and M. Zhou, *Ignition Desensitization of PBX via Aluminization.* Metallurgical and Materials Transactions A, 2015. **46**(10): p. 4578-4586.
21. Gresshoff, M. and C.A. Hrousis. *Probabilistic Shock Threshold Criterion*. in *14th International Detonation Symposium*. 2010. Coeur d'Alene, ID.
22. Welle, E.J., et al., *Microstructural effects on the ignition behavior of HMX.* Journal of Physics: Conference Series, 2014. **500**(5): p. 052049.
23. Walker, F.E. and R.J. Wasley, *Critical Energy for Shock Initiation of Heterogeneous Explosives.* Explosivstoffe, 1969. **17**: p. 9-13.
24. Yang, X., T. Zhou, and C. Chen, *Effective elastic modulus and atomic stress concentration of single crystal nano-plate with void.* Computational Materials Science, 2007. **40**(1): p. 51-56.
25. Hudson, R.J., P. Zioupos, and P.P. Gill, *Investigating the Mechanical Properties of RDX Crystals Using Nano-Indentation.* Propellants, Explosives, Pyrotechnics, 2012. **37**(2): p. 191-197.
26. Sewell, T.D., et al., *A molecular dynamics simulation study of elastic properties of HMX.* The Journal of Chemical Physics, 2003. **119**(14): p. 7417-7426.
27. James, H.R., *An extension to the critical energy criterion used to predict shock initiation thresholds.* Propellants Explosives Pyrotechnics, 1996. **21**(1): p. 8-13.
28. Gogulya, M.F., et al., *Mechanical sensitivity and detonation parameters of aluminized explosives.* Combustion Explosion and Shock Waves, 2004. **40**(4): p. 445-457.
29. Li, Y.-b., et al., *The effect of wax coating, aluminum and ammonium perchlorate on impact sensitivity of HMX.* Defence Technology, 2017. **13**(6): p. 422-427.
30. Gogulya, M., et al., *Explosive characteristics of aluminized HMX-based nanocomposites.* Combustion, Explosion, and Shock Waves, 2008. **44**(2): p. 198-212.

31. Gogulya, M.F., A.Y. Dolgoborodov, and M.A. Brazhnikov, *Fine structure of detonation waves in HMX-Al mixtures.* Chemical Physics Reports, 1998. **17**(1-2): p. 51-54.